J Mol Model (2017) 23: 273
DOI 10.1007/s00894-017-3441-6

ORIGINAL PAPER

Tetrahydroisoquinolines functionalized with carbamates as selective ligands of D2 dopamine receptor

Oscar Parravicini[1,3] · M. Lucrecia Bogado[2] · Sebastián Rojas[1] · Emilio L. Angelina[2] · Sebastián A. Andujar[1,3] · Lucas J. Gutierrez[1,3] · Nuria Cabedo[4,5] · M. Jesús Sanz[5,6] · M. Pilar López-Gresa[7] · Diego Cortes[4] · Ricardo D. Enriz[1,3]

Received: 26 January 2017 / Accepted: 15 August 2017 / Published online: 2 September 2017

Abstract A series of tetrahydroisoquinolines functionalized with carbamates is reported here as highly selective ligands on the dopamine D2 receptor. These compounds were selected by means of a molecular modeling study. The studies were carried out in three stages: first an exploratory study was carried out using combined docking techniques and molecular dynamics simulations. According to these results, the bioassays were performed; these experimental studies corroborated the results obtained by molecular modeling. In the last stage of our study, a QTAIM analysis was performed in order to determine the main molecular interactions that stabilize the different ligand-receptor complexes. Our results show that the adequate use of combined simple techniques is a very useful tool to predict the potential affinity of new ligands at dopamine D1 and D2 receptors. In turn the QTAIM studies show that they are very useful to evaluate in detail the molecular interactions that stabilize the different ligand-receptor complexes; such information is crucial for the design of new ligands.

Keywords THIQs functionalized with carbamates · Selective ligands of D2DR · Molecular modeling · QTAIM analysis

This paper belongs to Topical Collection QUITEL 2016

Electronic supplementary material The online version of this article (https://doi.org/10.1007/s00894-017-3441-6) contains supplementary material, which is available to authorized users.

✉ Ricardo D. Enriz
denriz@unsl.edu.ar

[1] IMIBIO-SL, CONICET, San Luis, Argentina

[2] IQUIBA-NEA, UNNE, CONICET, FACENA, Corrientes, Argentina

[3] IMIBIO-SL, CONICET, FQBF, UNSL, Chacabuco 915, 5700 San Luis, Argentina

[4] Dpto de Farmacología, Laboratorio de Farmacoquímica, Facultad de Farmacia, Universidad de Valencia, Valencia, Spain

[5] INCLIVA, University Clinic Hospital of Valencia, Valencia, Spain

[6] Dpto de Farmacología, Facultad de Medicina, Universidad de Valencia, Valencia, Spain

[7] Instituto de Biología Molecular y Celular de Plantas, Universitat Politècnica de València, CSIC, Ciudad Politécnica de la Innovación, Valencia, Spain

Introduction

Dopamine (DA), an important neurotransmitter in the mammalian central nervous system (CNS), is implicated in the control of different functions such as locomotor activity, emotional states, crucial cognitive functions, neuroendocrine secretions, and substance abuse disorders. DA also plays an important role in several psychiatric and neurological disorders affecting several million people worldwide. The actions of DA involve two receptor subtypes: DA 1-like receptors and DA 2-like receptors (D1DR and D2DR respectively). From a therapeutical point of view, drugs acting at D2DR are more relevant than those interacting with D1DR [1]. In this context, whereas the D1DR antagonists are used in the treatment of schizophrenia (antipsychotics), the agonists are used in the treatment of Parkinson's disease and depression [2, 3].

The critical importance of both D1DR and D2DR signaling in CNS function makes it highly desirable to gain detailed knowledge about the structural features necessary for full agonist activity and selectivity at these receptors. Dopamine receptors can be present in states of high affinity and such state has been shown to be associated with the functional state of the receptor that activates the G-protein and induces downstream cell signaling [4, 5].

A number of studies have been performed to determine the features important for the selectivity of either D1DR [6–9] or D2DR agonists [10–13]. For example, Tonani et al. [11] used vectors from the protonated nitrogen and hydrogen bonding heteroatom to dummy atoms representing the interaction points in the receptor. With this ligand-based pharmacophore modeling approach, it is possible to obtain discriminating models. Mottola et al. [6] published a D1DR pharmacophore model based on internal structural features such as the basic nitrogen atom and the oxygen atom of the meta-positioned hydroxyl group in the catechol. This study included a limited set of agonists together with a few inactive analogues; the inactive ones were used to define forbidden volumes. In addition, the D1DR and D2DR agonist selectivity has been studied by molecular electrostatic potentials (MEP) using density functional theory [14]. Wilcox et al. [15] carried out a D1/D2 agonist selectivity study by using various in silico methods such as comparative molecular field analysis (CoMFA), and homology and pharmacophore modeling.

In recent years, as part of our ongoing research program searching for new ligands for the D2DR dopamine, we have reported numerous compounds with different structural scaffolds. Thus, we report tetrahydroisoquinolines (THIQs) [16–19], protoberberines [20], and aminoindans [21] among others. Some of these compounds have shown some selectivity for D2DR with respect to the D1DR. More recently we reported three new series of compounds that are highly active and selective for the D2DR with respect to the D1. In this article, a molecular modeling study using combined techniques allowed us to explain the higher affinity for D2DR displayed by the compounds of this series [22].

On the other hand, the group at the University of Valencia has previously reported the synthesis of BTHIQs functionalized with carbamates [23]. These compounds possess moderate antibacterial and antifungal activities and they have no significant toxic effect. It should be noted that these compounds possess the pharmacophoric profile of the D2DR ligands, but they also have an extremely long side chain, when compared with traditional ligands of the D2DR. So we wonder whether this structural feature could encourage greater selectivity for the D2DR with respect to D1DR. There are different works in the literature that show that the different size of the hydrophobic pocket of the D1DR and D2DR could play a key role in the selectivity of the different ligands [24–26]. It is reasonable to think that the relatively large carbamate and linking portions of these compounds (denoted in red and green in Fig. 1) could be important to give selectivity to this series.

To answer this question we conducted a theoretical and experimental study on these. First we performed a molecular modeling study using combined techniques (docking and molecular dynamics simulations). In the second step we carried out bioassays in order to evaluate the biological activities. Finally we performed a QTAIM analysis on the most representative compounds of this series with the aim to evaluate in detail the molecular interactions that stabilize and destabilize the different complexes. The conclusions of our work are put forward in the last section.

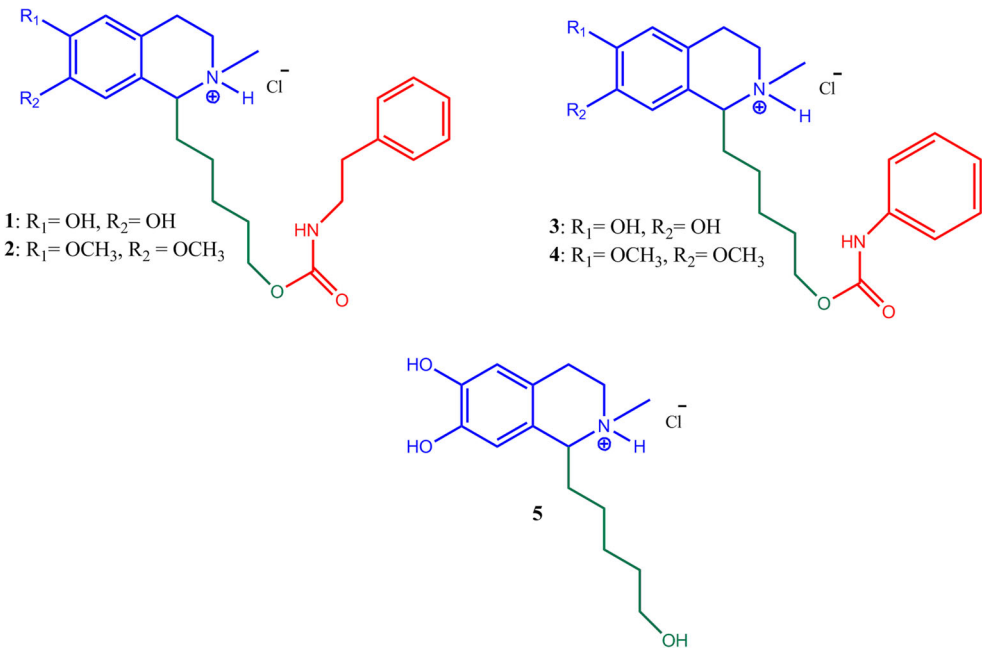

Fig. 1 Structures of the tested compounds

Methods

Computational details

Molecular docking and molecular dynamics approach

3D models of the human D1DR and D2DR were used for the molecular modeling study. Both models are based on the homology model from the crystallized D3DR, β2-adrenoceptor, and A2α adenosine receptor as templates. In fact, there are many molecular modeling studies in the literature, reporting D2DRs obtained by homology, all of them structurally very similar [27–29]. Thus, in the present study, we used two previously successful models to perform molecular modeling studies of different dopamine receptor ligands [22, 30, 31].

Carbamates and DR structures were converted from pdb to pdbqt format with MGLTools [32]. Molecular docking simulations were performed using the AutoDockVina software [32]. Several docking poses were considered and complexes with the lowest docking-energy according to the standard scoring function was regarded as the most favorable orientation and then used for MD calculations. To judge the validity of the docking poses previously reported experimental evidence was taken into account.

Antechamber Software in the AmberTools package was used to generate their parameters for MD simulations with FF99SB [33] and GAFF [34] force fields. All MD simulations were performed with the Amber 12 software package [35] (All-atoms force field FF99SB) using periodic boundary conditions for constant volume and cubic simulation cells. A steepest-descent algorithm for 1000 steps was used, in order to minimize the energy of each system. Next, the complexes were equilibrated during 500 ps at constant volume. The time step was 0.002 ps and the SHAKE [36] algorithm was applied. The systems were heated from 0 to 310 K and the temperature was controlled with Langevin [37] thermostat, collision frequency $\gamma = 5.0\ ps^{-1}$. Finally, after minimization and heating, three MD production simulations were conducted for each system at 300 K target temperature and extended to 10 ns overall simulation time. The particle mesh Ewald method (PME) [38] was applied using a grid spacing of 1.2 Å, a spline interpolation order of 4 and a real space direct sum cutoff of 10 Å — positional restraints were applied to all the backbone alpha carbons of the receptor. Post MD analysis was carried out with program PTRAJ.

In order to determine the residues of both D1DR and D2DR active sites involved in the complexes intermolecular interactions, a per-reside free energy decomposition analysis using the mm_pbsa program [39, 40] in AMBER 12 was performed. For mm_pbsa methodology, snapshots were taken at 10 ps time intervals from the corresponding last 5000 ps of the MD trajectory and the explicit water molecules were removed from the snapshots.

Topological analysis of the electron density distribution

Reduced 3D model systems of the D2DR selective compounds in complex with both D2DR and D1DR were constructed from the selected representative structures by keeping only receptor residues that interact directly with the ligands. These residues, that define the receptor binding pocket, were identified by using the free energy decomposition approach (MM/GBSA). Thus, the side chains of residues that contributed appreciably to the binding energy in the per residue energy decomposition were included in the reduced models.

The charge density of reduced model systems was then computed by DFT methodology with the PBE hybrid functional and 6-31G(d) as basis set, as implemented in Gaussian 09 package [41]. The topological analysis of charge density were performed in the context of the quantum theory of atoms in molecules (QTAIM) [42] with the help of Multiwfn software [43].

In an attempt to capture some of the complex system dynamics, the QTAIM analysis was performed on several frames extracted from the MD trajectories. Concretely, MD trajectories were first clustered by the root mean square deviation (RMSD) of the protein backbone atoms employing the cluster tool implemented in Amber package [44]. Then, the representative structures from the three most populated clusters were selected for the QTAIM analysis. The reported charge density values correspond to the average over the three selected cluster representative structures.

Experimental

Synthesis

Compounds 1–5 were obtained according to reference [23].

Binding assays

Binding experiments were performed on striatal membranes. Each striatum was homogenized in 2 mL ice-cold Tris-HCl buffer (50 mM, pH = 7.4 at 22 °C) with a Polytron (4 s, maximal scale) and immediately diluted with Tris buffer. The homogenate was centrifuged either twice ([^{3}H] SCH 23390 binding experiments) or four times ([^{3}H] raclopride binding experiments) at 20,000 g for 10 min at 4 °C with resuspension in the same volume of Tris buffer between centrifugations. For [^{3}H] SCH 23390 binding experiments, the final pellet was resuspended in Tris buffer containing 5 mM $MgSO_4$, 0.5 mM EDTA and 0.02% ascorbic acid (Tris-Mg buffer), and the suspension was briefly sonicated and diluted to a protein concentration of 1 mg/mL. An aliquot of 100 μL of freshly prepared membrane suspension (100 μg of striatal protein) was incubated for 1 h at 25 °C with 100 μL Tris buffer containing [^{3}H] SCH 23390 (0.25 nM final concentration) and 800 μL of Tris-Mg buffer containing the required drugs. Non-specific binding was

determined in the presence of 30 μM SK&F 38393 and represented around 2–3% of total binding. For [^{3}H] raclopride binding experiments, the final pellet was resuspended in Tris buffer containing 120 mM NaCl, 5 mM KCl, 1 mM $CaCl_2$, 1 mM $MgCl_2$, and 0.1% ascorbic acid (Tris-ions buffer), and the suspension was treated as described above. A200 μL aliquot of freshly prepared membrane suspension (200 μg of striatal protein) was incubated for 1 h at 25 °C with 200 μL of Tris buffer containing [^{3}H] raclopride (0.5 nMfinal concentration) and 400 μL of Tris-ions buffer containing the drug being investigated. Non-specific binding was determined in the presence of 50 μM apomorphine and represented around 5–7% of total binding. In both cases, incubations were stopped by addition of 3 mL of ice cold buffer (Tris-Mg buffer or Tris-ions buffer, as appropriate) followed by rapid filtration through Whatman GF/B filters using a Brandel harvester (model M − 24, Biochemical Research and Development Laboratories, Inc.). Tubes were rinsed with 3 mL ice cold buffer, and filters were washed with 3 × 3 mL ice-cold buffer. After the filters had been dried, radioactivity was counted in 4 mL scintillation liquid (Optiphase 'Hisafe' 2, Perkin Elmer). Filter blanks corresponded to approximately 0.5% of total binding and were not modified by drugs.

Results and discussion

Molecular modeling

In the first stage of our study, we performed an exploratory study using docking calculations and then molecular dynamics (MD) simulations. For this study, compounds 1–5 (Fig. 1) previously reported in reference [23] were selected. Our results predict that these compounds could bind to the active site of D1DR and D2DR in a manner quite similar to that of other ligands reported by our group [16–18, 30, 45]. Note that the pharmacophoric group of these compounds is spatially accommodated in exactly the same way as dopamine [46] and the other previously studied ligands [18, 20, 22, 31]. Then we perform the analysis per residue of compounds 1 and 3 in both D1DR and D2DR, in order to compare them (Fig. 2). The residues were numbered according to the Ballesteros-Weinstein numbering scheme [47, 48]. On the analysis of these histograms, it is evident that both compounds 1 and 3 would show a significantly greater affinity for D2DR than for D1DR (compare Figs. 2a with 2b and 3a with 3b).

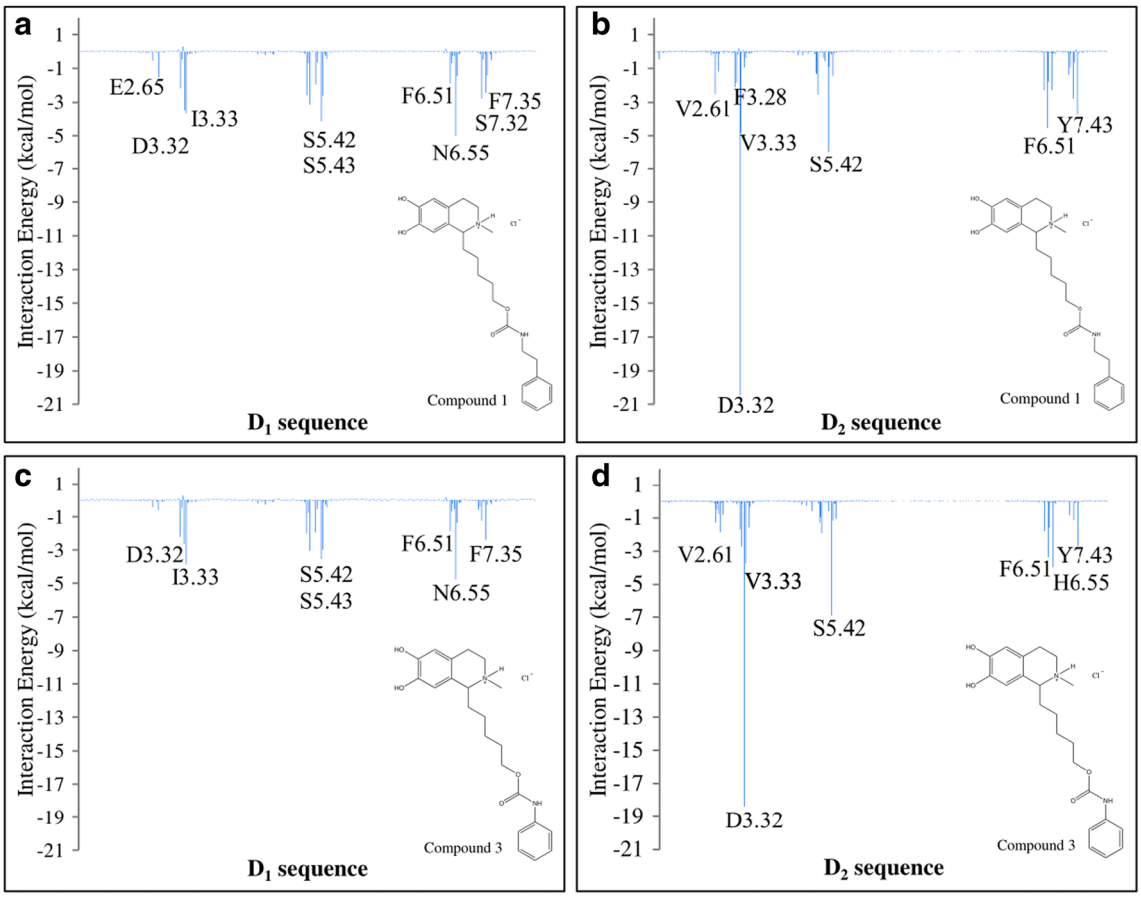

Fig. 2 Histograms of interaction energies of partitioned amino acids for D1DR and D2DR when complexed with compounds 1 (a, b) and 3 (c, d). The *x-axis* denotes the residue number of DR and the *y-axis* shows the interaction energy between the compound and the specific residue. Negative and positive values represent favorable or unfavorable binding, respectively

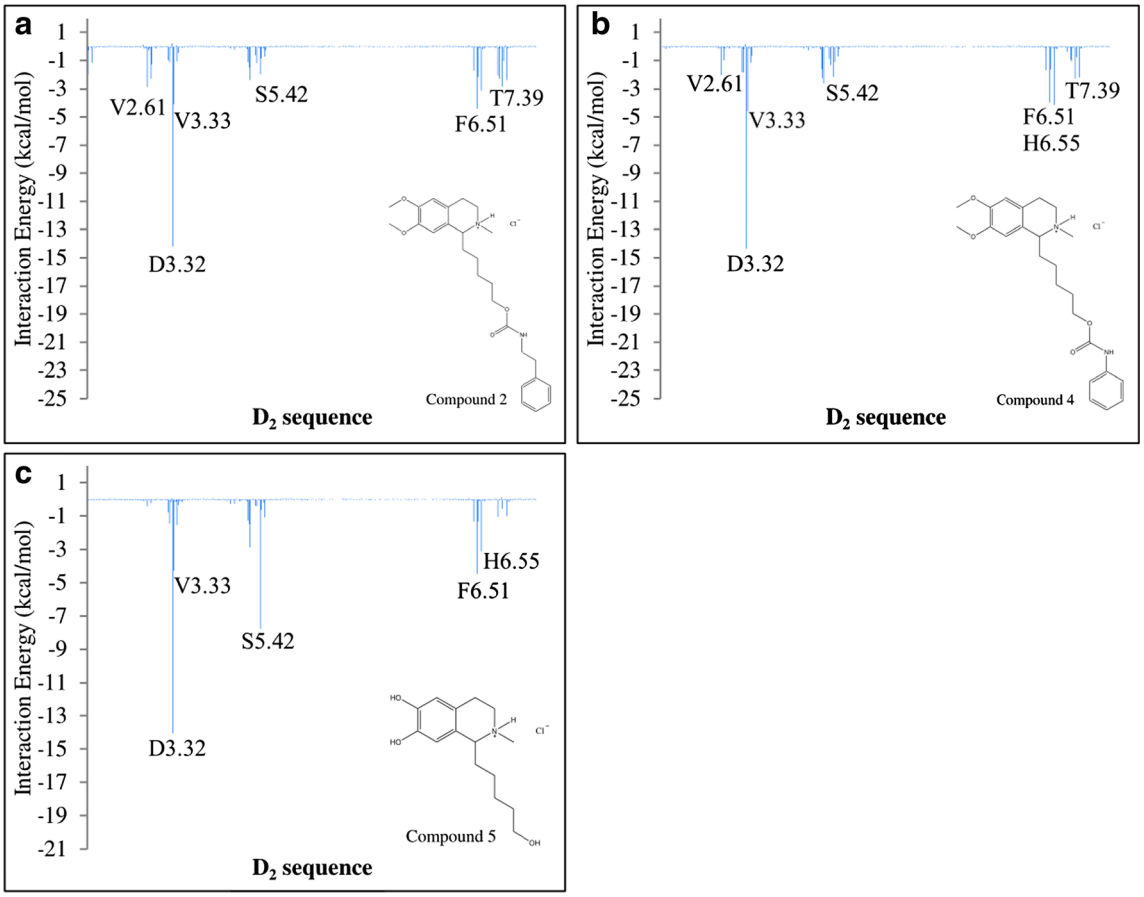

Fig. 3 Histograms of interaction energies partitioned for D2DR amino acids when complexed with compound 2 (a); compound 4 (b) and compound 5 (c). The *x-axis* denotes the residue number of DR and the *y-axis* shows the interaction energy between the compound and the specific residue. Negative and positive values represent favorable or unfavorable binding, respectively

We also analyzed the histograms obtained for compounds 2, 4, and 5 at the D2DR. As we expected, the interactions of compounds 2 and 4 are significantly weaker than those of their counterparts 1 and 3 (Fig. 3). As we have seen in other series of compounds, methoxylated derivatives have weaker interactions with $S_{5.43}$ and $S_{5.46}$, which makes interactions of the pharmacophoric group weaker for these compounds. Compound 5, whose side chain is markedly shorter than that of the rest of the derivatives studied, shows a histogram comparable to that of compounds 1 and 3. However, MD simulations predict that the interactions for compound 5 are weaker than those obtained for compounds 1 and 3.

The histograms obtained for compounds 1 and 3 are very similar to those of the most active compounds from other previously reported series [20, 22]. Further, our results predict that these compounds could be highly selective for the D2DR with respect to D1DR. Thus, these results are very promising with respect to the potential selectivity of compounds 1 and 3 by the D2DR relative to D1DR. On the basis of these results we decided to test them as ligands of both D1DR and D2DR. We also included compounds 2, 4, and 5 in the bioassays as controls. In the particular case of compounds 2 and 4 as compounds which should be less active than their counterparts 1 and 3, respectively.

Experimental corroboration

Compounds 1–5 have been previously reported in reference [23] and their synthesis is explained in detail. The compounds were synthesized according to reference [23]. Once compounds 1–5 were synthesized, they were all evaluated using the bioassay described in the experimental section. Interestingly, compounds 1 and 3 showed a very strong and selective activity on the D2DR with respect to the D1DR (Table 1). It is important to note that compounds 1 and 3 are among the most selective compounds we have reported to date.

On the other hand and as we expected, compounds 2 and 4 showed a markedly lower affinity for both D1 and D2 receptors. Compound 5 showed a significant affinity for D2DR, although this effect is lower than those found for compounds 1 and 3. These experimental results are in complete agreement with the molecular modeling. These results show that these exploratory studies may be very useful in predicting the

Table 1 Affinity values (Ki) and selectivity ratios obtained for the assayed compounds

Compound	Ki_{D1DR} (μM)	Ki_{D2DR} (μM)	Ki_{D1DR}/Ki_{D2DR}
1	0.811	0.151	5.371
2	12.440	0.762	16.325
3	0.466	0.091	5.121
4	17.490	24.440	0.716
5	0.967	0.338	2.861

different affinities of ligands on both D1DR and D2DR, even before the synthesis of such compounds.

At this stage of our study we were particularly interested in knowing the main molecular interactions that stabilize and destabilize the different ligand-receptor (L-R) complexes. In previous studies [19, 20, 22, 31, 46, 49, 50] we demonstrated the usefulness of QTAIM analysis to evaluate the molecular interactions involved in the L-R junction, therefore in the final step of our study we performed a QTAIM study of compounds 1–5, the results of which are discussed in the next section.

QTAIM analysis

Specificity determinants for D2DR binding

One of the advantages of the QTAIM methodology over other global measures of the interaction energy is that it allows one to decompose the interaction energy in contribution by atom or group of atoms, which makes it particularly useful in analysis, design and optimization of ligand molecules. Accordingly, for the QTAIM analysis we partitioned the compounds in three substructures, as indicated in Fig. 1. Substructure in blue resembles dopamine and can be considered as the "pharmacophore" for these receptors; the carbamate moiety is depicted in red and the linker that connects both, pharmacophore and carbamate is highlighted in green.

Figure 4 shows in stacked bars the sum of the charge density values at the intermolecular bond critical points (BCPs) for complexes of compounds 1 and 3 with D1DR and D2DR. The contributions of pharmacophore, linker, and carbamate to the overall anchoring strength of compounds at the receptor binding pocket are depicted with different colors. The charge density sums were averaged over three cluster representative structures selected from the MD trajectories.

As depicted in Fig. 4 the charge density sum for both compounds are higher in D2DR than in D1DR which indicates that they are more strongly anchored to D2DR binding pocket than to D1DR. This trend is in agreement with experimental affinity values for these compounds. Of the three parts that make up compounds 3 and 1, the pharmacophore is the one with the greatest contribution to the overall anchoring strength in both D1DR and D2DR. Moreover, in both compounds the pharmacophore contributes in about the same magnitude to the overall anchoring in both receptor subtypes. This finding is in line with previous experimental evidence that show that dopamine binds with almost the same affinity to both receptor subtypes (Ki_{D1DR} 0.550 μM versus Ki_{D2DR} 0.560 μM, see reference Parraga et al. [22]).

The overall binding modes of compounds 3 and 1 in both receptors sub-types are shown in Figs. 5 and 6, respectively. In these figures, clusters representative of structures of the compound in both receptor sub-types were superposed by their backbone atoms. Only some structural elements in the superposition are shown for easy viewing. Since we used the Ballesteros-Weinstein numbering scheme any residue occupying an equivalent position along the trans-membrane segments bears the same numbering in both receptor sub-types so that they can be directly compared.

Note in Figs. 5a and 6a that pharmacophore of compounds 3 and 1 respectively adopts the same binding mode within each receptor sub-type (i.e., in the three cluster representative structures). However, when binding modes of pharmacophore in D2DR is compared with that of D1DR strong differences can be observed.

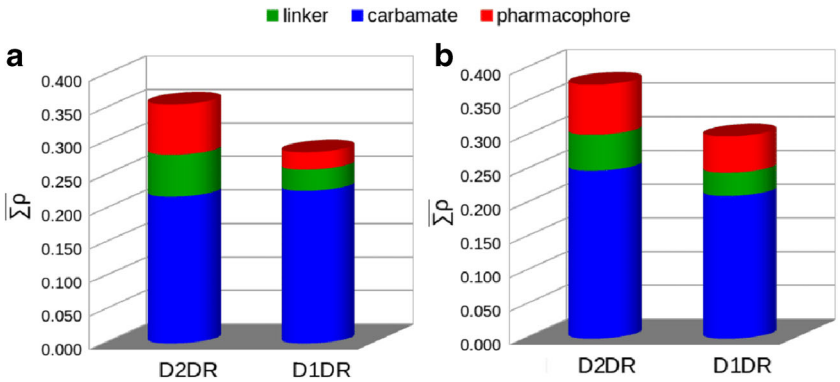

Fig. 4 Sum of the charge density values (in atomic units) at the intermolecular bond critical points (BCPs) for complexes of compounds **3** (a) and 1 (b) with D1DR and D2DR. The expressed values were obtained by averaging the charge density sum for each contribution (i.e., pharmacophore, linker and carbamate) over the three cluster representative structures extracted from the MD trajectories

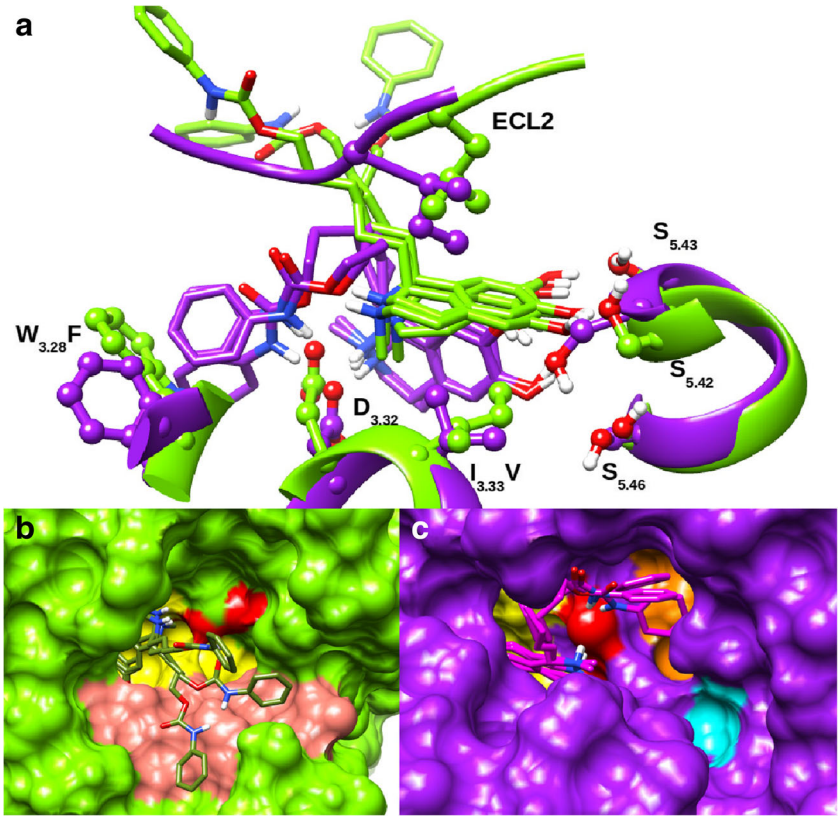

Fig. 5 Backbone superposition of the three representative structures selected from MD simulations of compound 3 in D1DR (green) and D2DR (purple). Only some structural elements in the superposition are shown for easy viewing. In top panel the key structural elements that determine the different binding mode of compound 3 in both receptor sub-types are shown (a). In bottom panels the conformations of compound 3 on molecular surfaces of D1DR (b) and D2DR (c), are shown separately. Pharmacophore binding sub-pocket is depicted in yellow. Carbamate binding sub-pockets are depicted in orange, cyan, and pink. Surface over D3.32 is depicted in red

Figures 7 and 8 shows the network of interactions of compounds 3 and 1, in both receptor sub-types. The molecular graphs were constructed from one of the cluster representative structures shown in Figs. 5 and 6.

Consistent with previous experimental and theoretical data [22], the simulations indicated the relevance of negatively charged aspartate 3.32 for D2DR and D1DR ligand binding. As can be seen in Figs. 5 and 6, the pharmacophore protonated

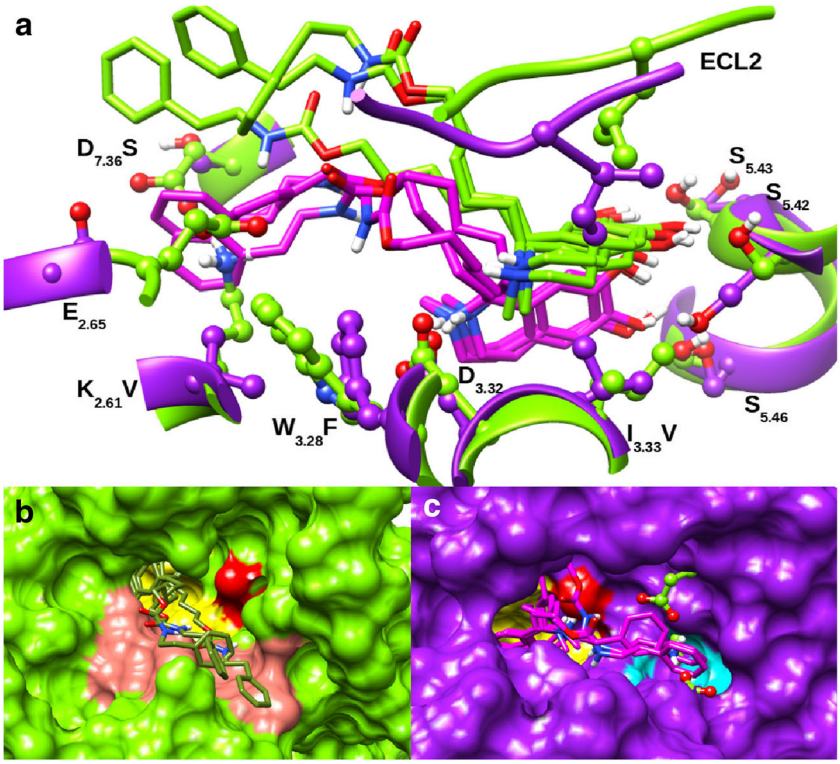

Fig. 6 Backbone superposition of the three representative structures selected from MD simulations of compound 1 in D1DR (green) and D2DR (purple). Only some structural elements in the superposition are shown for easy viewing. In the top panel the key structural elements that determine the different binding mode of compound 1 in both receptor sub-types are shown (a). In bottom panels the conformations of compound 1 on molecular surfaces of D1DR (b) and D2DR (c), are shown separately. Pharmacophore binding sub-pocket is depicted in yellow. Carbamate binding sub-pockets are depicted in cyan and pink. Surface over D3.32 is depicted in red

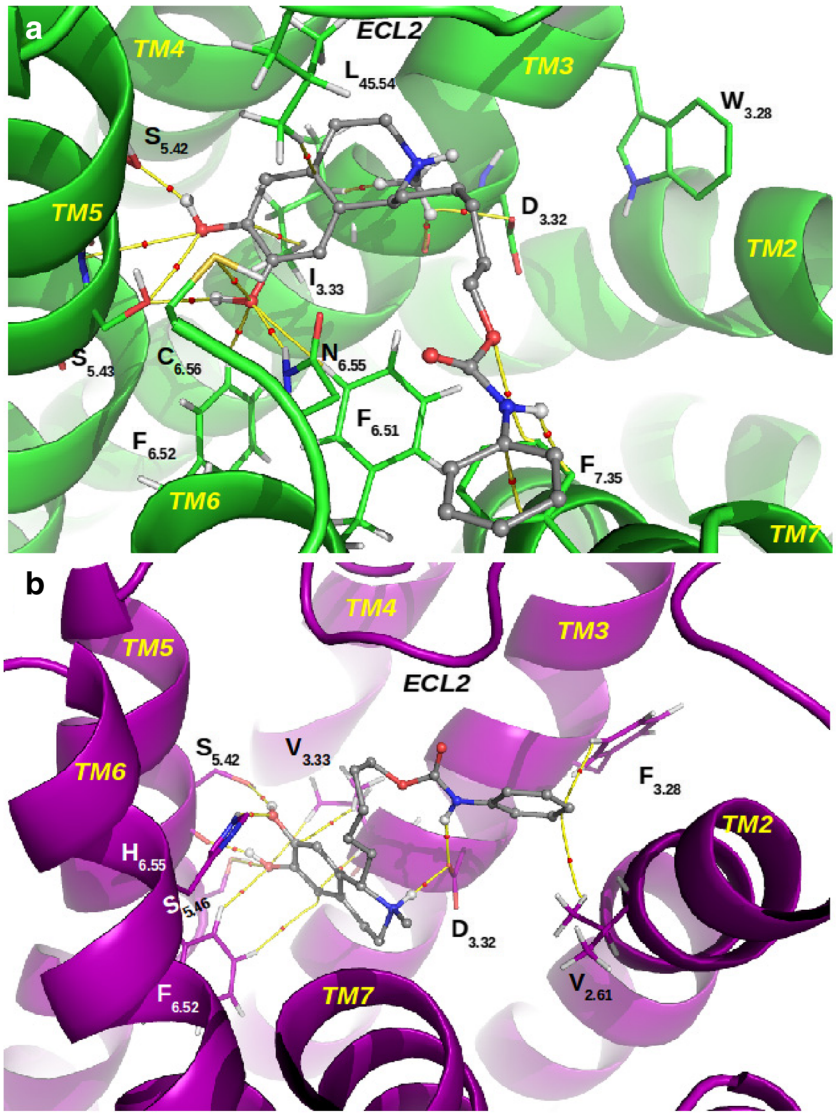

Fig. 7 Spatial view of complexes of compound 3 with DRD1 (a) and DRD2 (b) constructed from a cluster representative structure. Topological elements of the charge density as well as structural elements are depicted. Yellow lines connecting the nuclei are the bond paths, and the small red spheres on them are the bond critical points (BCPs). Ligand atoms are depicted in gray

amine group of compounds 3 and 1 is in close position to interact with $D_{3.32}$, in both D1DR and D2DR receptor subtypes. However, the molecular graphs in Figs. 7 and 8 reveal that direct strong interactions between ammonium proton and highly conserved $D_{3.32}$ only occurs in D2DR. In D1DR the N-methyl substituent prevents the direct interaction of the amine proton with $D_{3.32}$. In consequence, ligand anchoring to $D_{3.32}$ is much weaker in D1DR ($\Sigma\rho_3$ = 0.0248 a.u., $\Sigma\rho_1$ = 0.0283 a.u.) than in D2DR ($\Sigma\rho_3$ = 0.0866 a.u., $\Sigma\rho_1$ = 0.0800 a.u.).

Moreover, in D2DR the catecholic ring of 3 and 1 is stacked vertically between residues $V_{3.33}$ and $F_{6.52}$. Bond paths connecting hydrogen atoms of $V_{3.33}$ and $F_{6.52}$ to the pharmacophore ring carbon atoms can be observed. As a consequence of this interaction pattern the plane of the catecholic ring is oriented parallel to the central axis of the transmembrane helices bundle. On the other hand in D1DR the same ring of 3 and 1 orients perpendicularly to the central axis of the receptor. This is in part due to the substitution of $V_{3.33}$ by a bulkier isoleucine ($I_{3.33}$V) which does not leave enough room between $I_{3.33}$ and $F_{6.52}$ and so the catecholic ring in D1DR lies over $I_{3.33}$. In the superposition shown in Figs. 5a and 6a, it can be seen that the $I_{3.33}$ side chain from D1DR (green) would crash with the pharmacophore catecholic ring if it were to anchor in D1DR as it actually does in D2DR (purple).

Another determinant for the differential binding mode of pharmacophore in D2DR and D1DR is the extracellular loop 2 (ECL2) which is on top of the receptor binding pocket. In D2DR the segment of ECL2 between TM5 and the conserved cysteine that usually form a disulfide bond with TM3 extends further inside/down the binding pocket not leaving enough space for the pharmacophore to adopt a D1DR-like binding mode. This is evidenced in Figs. 5a and 6a that show how the ECL2 residues from D2DR (purple) would prevent compounds 3 and 1 to adopt the conformations they have in D1DR (green) due to steric clashes with pharmacophore as well as carbamate atoms.

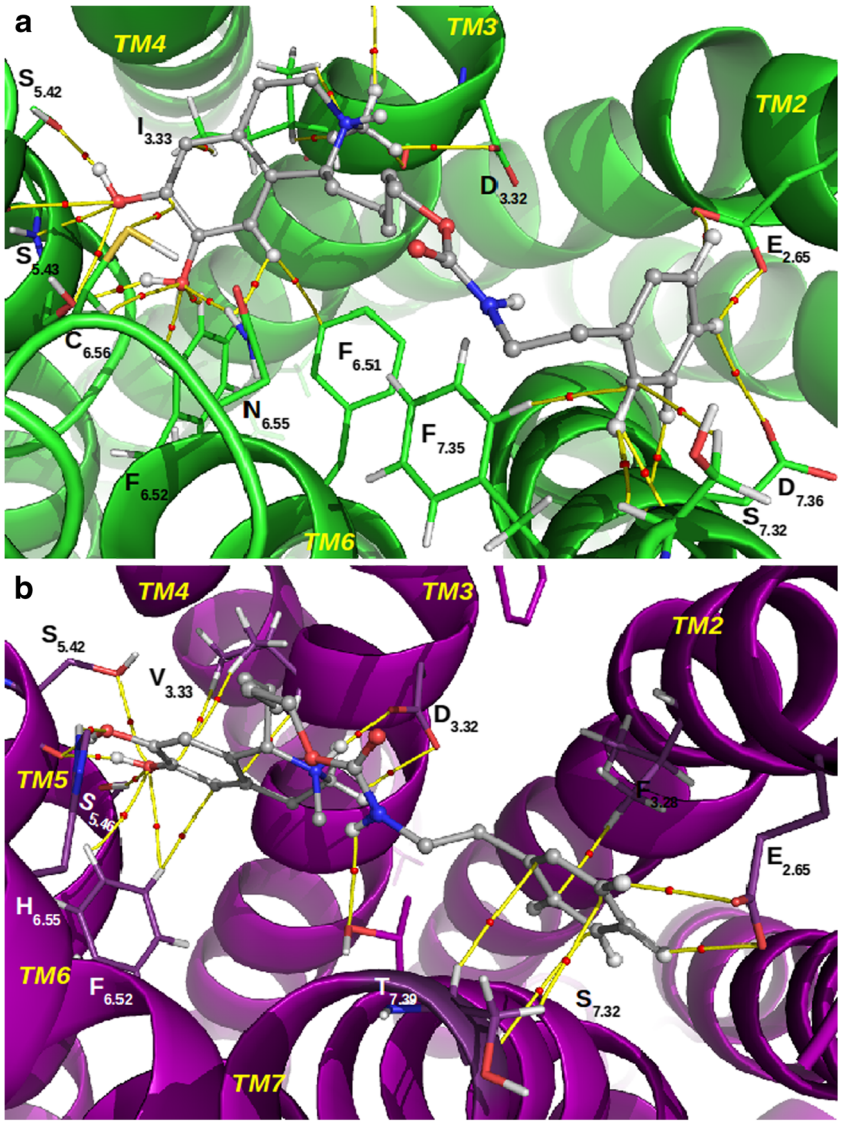

Fig. 8 Spatial view of complexes of compound 3 with DRD1 (a) and DRD2 (b) constructed from a cluster representative structure. Topological elements of the charge density as well as structural elements are depicted. Yellow lines connecting the nuclei are the bond paths, and the small red spheres on them are the bond critical points (BCPs). Ligand atoms are depicted in gray

As a consequence of the distinct binding mode of the pharmacophore in both receptor subtypes, a different interaction pattern of the catecholic OH groups is also observed.

In D1DR the *meta* and *para* hydroxyl hydrogen atoms of 3, i.e., *meta*-H and *para*-H, are hydrogen bonded to $S_{5.42}$ and $S_{5.43}$, respectively. While the oxygen atoms of the catecholic OH groups are connected through bond paths to $F_{6.51}$, $F_{6.52}$, $N_{6.55}$, $C_{6.56}$, $S_{5.42}$, and $S_{5.43}$ (see Fig. 7).

On the other hand, in D2DR the *meta*-H and *para*-H atoms of 3 are hydrogen bonded to carbonyl and hydroxyl oxygen atoms of $S_{5.42}$, respectively but not direct interaction with $S_{5.43}$ is observed. Instead, a new oxygen-oxygen interaction between *meta*-O and the hydroxyl oxygen atom of $S_{5.46}$ that is one turn below $S_{5.42}$, is established (see Fig. 4). In addition, *meta*-O and *para*-O atoms also form interactions with residues $V_{3.33}$, $I_{5.33}$, $F_{6.52}$, and $H_{6.55}$. Similar interaction pattern can be observed in Fig. 8 for pharmacophore of compound 1 in both receptor sub-types.

Added together, the interactions of the *meta*-OH and *para*-OH groups of 3 and 1 are stronger in D1DR ($\Sigma\rho_3 = 0.1062$ a.u., $\Sigma\rho_1 = 0.1192$ a.u.) than in D2DR ($\Sigma\rho_3 = 0.0851$ a.u., $\Sigma\rho_1 = 0.1118$ a.u.). This compensates the weaker interactions with $D_{3.32}$ in the first receptor subtype so that the pharmacophore is anchored to both receptor binding pockets with almost the same strength.

Since the pharmacophore is anchored with equal strength to both receptor subtypes it does not explain by itself the difference in binding strength of 3 and 1 to D1DR and D2DR. However, as discussed above, this is the part of compounds that binds most strongly to receptor binding pocket and so it controls the binding mode of the entire ligand. Given that the binding mode of the pharmacophore is markedly different in both receptor subtypes, it might explain at least in part why the placement of the carbamate moiety into the receptor binding site is also very different in both cases.

As shown in Fig. 4, the carbamate as well as the linker of 3 and 1 binds more strongly to the binding pocket of D2DR than D1DR, which explains the overall stronger binding of these compounds to D2DR.

Unlike pharmacophore binding, there are marked differences in the binding mode and interaction networks of carbamate of compounds 3 and 1 in both receptor sub-types. Therefore, they are discussed separately.

Compound 3

Figure 5 gives some clues about the origin of the stronger anchoring of carbamate in D2DR. Note in Fig. 5a that in D2DR the carbamate adopts a unique binding mode in the three cluster representative structures where it is firmly anchored to the negatively charged $D_{3.32}$ residue. On the other hand, in D1DR the carbamate anchoring to $D_{3.32}$ does not occur, instead it moves almost freely inside D1DR binding pocket.

By comparing Fig. 5b, c it can be seen that in complex 3 with D2DR the carbamate phenyl ring lies in a sub-pocket (in orange) that is absent in complex 3 with D1DR. At the bottom of that D2DR sub-pocket there is a phenylalanine in position 3.28 that in D1DR is occupied by a bulkier tryptophan. As a consequence of that substitution the sub-pocket is occluded in D1DR and therefore the carbamate cannot be anchored to it, in the way it does in D2DR. Also note in the superposition of Fig. 5a that the presence of the bulkier $W_{3.28}$ in D1DR (green) would cause steric clashes with the carbamate moiety if it were anchored to $D_{3.32}$, as it actually does in D2DR (purple).

Thus, the $W_{3.28}F$ substitution together with a different pharmacophore anchoring might explain why the carbamate cannot interact with $D_{3.32}$ in D1DR.

Figure 7 shows the network of interactions of the carbamate moiety from compound 3 in both D1DR and D2DR binding pockets. Some of the topological elements that connect carbamate to binding site were removed for easy viewing. As seen in Fig. 7, in complex 3 with D2DR the carbamate amide proton as well as the pharmacophore ammonium proton is connected through bond paths to the carboxyl oxygen atoms of $D_{3.32}$. On the other hand, in D1DR no interactions between ligand atoms and $D_{3.32}$ are formed, except for the weak contacts with the methyl group substituting the pharmacophore nitrogen atom. The lack of interactions of the carbamate with $D_{3.32}$ explains in part why this group is poorly anchored to the binding pocket of D1DR. Another reason for a weaker carbamate linkage in D1DR than in D2DR is related to distinct topography of the binding pocket in each case. In D2DR the carbamate phenyl ring occupies a hydrophobic binding sub-pocket that is buried in the TMs bundle (Fig. 5c) and so, it forms several interactions with surrounding hydrophobic residues. On the other hand, in D1DR the carbamate moiety lies over an extended solvent exposed surface depicted in pink in Fig. 5b where the intermolecular interactions can be formed only with one of the faces of the carbamate. Figure S1 in Supporting information shows the entire set of bond critical points (BCPs) and bond paths that connect the carbamate to receptor binding pocket. As can be seen in that figure, the network of interactions is quite more intricate in D2DR than in D1DR.

Compound 1

Similarly to compound 3, the carbamate moiety of compound 1 binds to D1DR in the flat solvent exposed surface depicted in pink in Fig. 3b. However, unlike compound 3, when 1 binds to D2DR the carbamate does not form any interaction with $D_{3.32}$. This could be due to the longer carbamate N-phenyl ethyl group of compound 1 which would not fit into the binding sub-pocket that is otherwise occupied by the N-phenyl group of compound 3 (note that this binding sub-pocket is absent in complex of compound 1 with D2DR since the $F_{3.28}$ at the bottom of the sub-pocket tends to interact with the nearby $D_{3.32}$ when it is empty, thus occluding its entrance (Figs. 5c and 6c)).

Instead, carbamate moiety of 1 is anchored in a deep sub-pocket limited by residues $Y_{1.35}$, $L_{1.39}$, $V_{2.61}$, $L_{2.64}$, $E_{2.65}$, $S_{7.36}$, $T_{7.39}$, $W_{7.40}$, and $Y_{7.43}$ which is depicted in cyan in Fig. 6c. This sub-pocket is not formed in D1DR because residues $V_{2.61}$ and $S_{7.36}$ are substituted in D1DR by lysine and aspartate respectively, which form a salt bridge that occlude the sub-pocket entrance (see Fig. 6c). Also note in the superposition of Fig. 6a that the presence of this salt bridge would cause steric clashes with the carbamate moiety if it were anchored as it is in D2DR (in purple). Instead, in D1DR the carbamate group (in green) is anchored on top of the salt bridge.

The molecular graph in Fig. S2 shows the entire set of intermolecular interactions established by the carbamate moiety of compound 1 in both receptor sub-types. As evidenced in that figure the network of interactions is more intricate in D2DR than in D1DR which is in line with the fact that in D2DR the carbamate is anchored in a deep binding sub-pocket in the transmembrane helices bundle as opposed to the flat solvent exposed surface on which it is anchored to D1DR. As a result of the more intricate network in D2DR the carbamate moiety is more strongly anchored to this receptor sub-type than to D1DR. Moreover, the substitution of $V_{7.39}$ in D1DR by the more polar threonine in D2DR also contributes to the stronger anchoring of the carbamate in this last receptor sub-type. Note in Figs. 5 and S2 that in D2DR the $T_{7.39}$ hydroxyl oxygen atom forms a hydrogen bond with carbamate amide proton which cannot be formed by $V_{7.39}$ in D1DR.

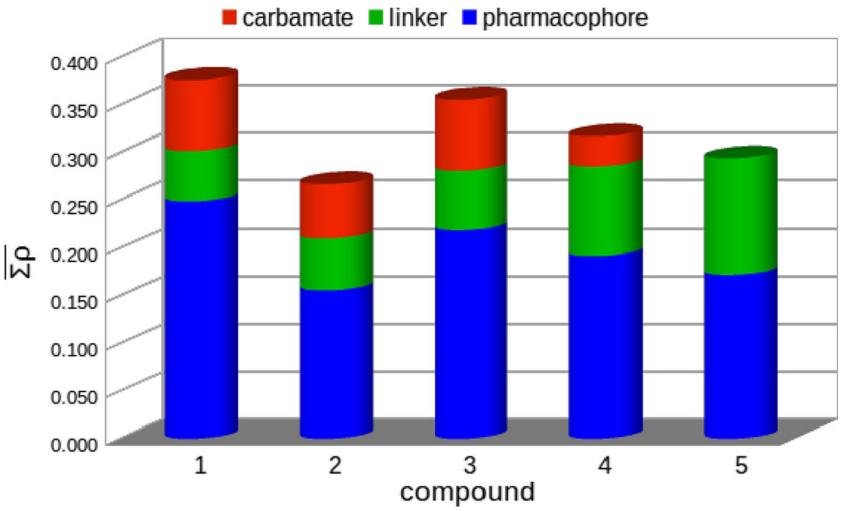

Fig. 9 Sum of the charge density values (in atomic units) at the intermolecular bond critical points (BCPs) for complexes of compounds 1, 2, 3, 4, and 5 with D2DR. The expressed values were obtained by averaging the charge density sum for each contribution (i.e., pharmacophore, linker, and carbamate) over the three cluster representative structures extracted from the MD trajectories

Affinity determinants for D2DR binding

Figure 9 shows in stacked bars the sum of charge density values at the intermolecular bond critical points (BCPs) for complexes of D2DR with compounds 1 and 3 and their methylated counterparts 2 and 4, respectively. Also the charge density sum for complex 5/D2DR is shown, in which compound 5 lacks the carbamate group.

By comparing compounds 1 and 3 with their counterparts 2 and 4, respectively, it becomes evident that OH methylation at the catecholic OH groups decreases the overall binding strength of these compounds to D2DR which is in line with the experimental observations (Table 1).

Figure 10 shows the backbone superposition of complexes of compounds 3 and 4 with D2DR. Similar differences are observed in the superposition of compounds 1 and 2 (not shown).

As seen in Fig. 10, the pharmacophore adopts the same binding mode in both hydroxylated and methoxylated complexes. However, as evidenced in Fig. 9 the pharmacophore interactions weaken on going from complex of compounds 1, 3 to those of the methylated analogs 2, 4, respectively. The weakening is mostly due to the interactions of the catecholic hydroxyl groups with conserved serine residues at TM5 which are lost (or weakened) after OH methylation.

One of the key interactions that are lost due to OH methylation involves the backbone oxygen of $S_{5.42}$ and catecholic hydroxyl hydrogen atom in *meta* position of compounds 1, 3 (see Figs. 7b, 8b). Besides its contribution to ligand anchoring, this interaction also modifies the architecture of TM5 because it causes the rupture of an intra-TM5 hydrogen bond in which $S_{5.42}$ carbonyl oxygen is involved. This is reflected in the secondary

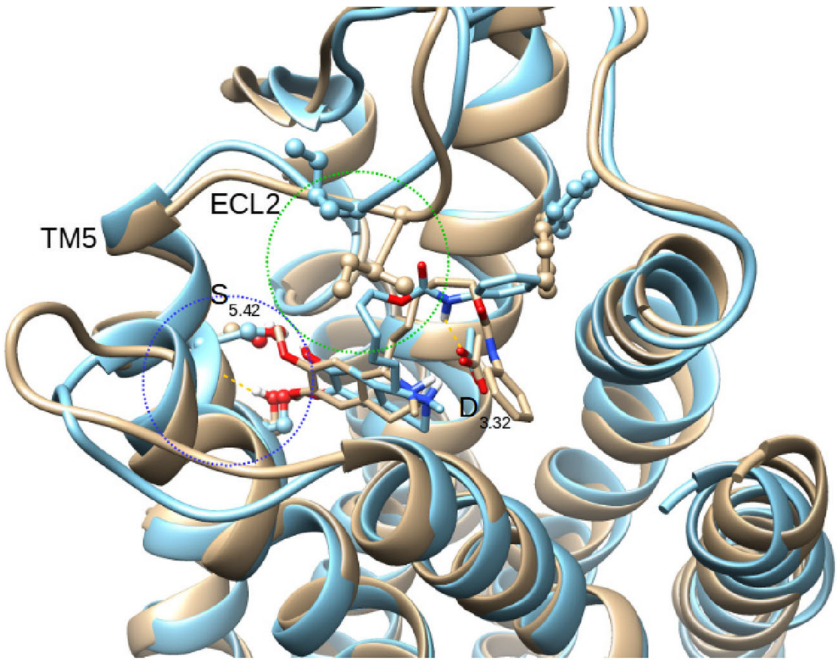

Fig. 10 Backbone superposition of complexes of compounds 3 (light blue) and 4 (gray) with D2DR

structure of TM5 that is locally deformed around $S_{5.42}$ in complex 3/D2DR but remains intact in complex 4/D2DR (see Fig. 10).

It has already been argued that ligand interaction with backbone of $S_{5.42}$ influences the folding of the outer (extracellular) segment of TM5 and adjacent ECL2 loop [51]. In line with this arguing, note in Fig. 10 how ECL2 in complex 4/D2DR extends further down the binding pocket entrance as compared with ECL2 of complex 3/D2DR. Moreover, note in Fig. 10 that ECL2 residues mostly interact with the linker part of compounds.

In order for both pharmacophore and linker to be hydrogen bonded to the same negatively charged residue $D_{3.32}$, the linker has to adopt the curved up conformation it has in complex 3/D2DR. However, this "curved up" conformation of linker is not allowed in complex 4/D2DR because it would crash with ECL2 that protrudes into the binding pocket to a greater extend in this complex. As a result, carbamate group is no longer hydrogen bonded to $D_{3.32}$ in complex 4/D2DR (Fig. 10). The loss of this interaction explains at least in part the lower contribution of carbamate to total anchoring strength due to OH methylation (see Fig. 9).

Conclusions

We report here a new series of highly selective ligands on the D2DR. Our molecular modeling study predicted that a series of THIQs functionalized with carbamates could be selective ligands on the D2DR receptors with respect to D1DR. Our experimental results confirmed the predictions of the modeling studies, showing the importance of this type of exploratory analysis before performing the syntheses and bioassays.

To complete our study, we performed a QTAIM study for the five compounds of this series in order to evaluate the molecular interactions stabilizing the different complexes. This study made it possible to explain clearly why these compounds are highly selective on the D2DR. Our results indicate that the relatively long portion formed by the connecting chain and carbamate group can be accommodated spatially much better in the D2DR than in the D1DR.

On the other hand the QTAIM study also allowed us to explain why the methoxylated derivatives (compounds 2 and 4) have much less affinity for both receptors than the hydroxylated compounds (compounds 1 and 3). In this case the important hydrogen bond network of the pharmacophoric group is affected by the replacement of OH function by OCH_3.

Our results show that the adequate use of combined simple techniques is a very useful tool to predict the potential affinity of new ligands at dopamine D1 and D2 receptors. On the other hand, the QTAIM studies prove once more how useful they are to evaluate in detail the molecular interactions that stabilize the different ligand-receptor complexes. This information is crucial as an element for the design of new ligands on this type of receptors.

Acknowledgements This work was supported by Universidad Nacional de San Luis (UNSL) and CONICET grants 2-1214 and PIP444, respectively. E.L.A, L.J.G, S.A.A and R.D.E are staff members of the National Scientific and Technical Research Council - Argentina (CONICET, Argentina). The authors would like to thanks MSc. Daniel O. Zamo for technical assistance (CONICET-Argentina).

References

1. Beaulieu JM, Gainetdinov RR (2011) The physiology, signaling, and pharmacology of dopamine receptors. Pharmacol Rev 63(1): 182–217. https://doi.org/10.1124/pr.110.002642
2. Luthra PM, Kumar JBS (2012) Plausible improvements for selective targeting of dopamine receptors in therapy of Parkinson's disease. Mini-Rev Med Chem 12(14):1556–1564. https://doi.org/10.2174/138955712803832645
3. Poewe W (2009) Treatments for Parkinson disease-past achievements and current clinical needs. Neurology 72 (7 SUPPL. 2): S65-S73. https://doi.org/10.1212/WNL.0b013e31819908ce
4. Seeman P, Watanabe M, Grigoriadis D (1985) Dopamine D2 receptor binding sites for agonists: a tetrahedral model. Mol Pharmacol 28(5):391–399
5. McDonald WM, Sibley DR, Kilpatrick BF, Caron MG (1984) Dopaminergic inhibition of adenylate cyclase correlates with high affinity agonist binding to anterior pituitary D2 dopamine receptors. Mol Cell Endocrinol 36(3):201–209. https://doi.org/10.1016/0303-7207(84)90037-6
6. Mottola DM, Laiter S, Watts VJ, Tropsha A, Wyrick SD, Nichols DE, Mailman RB (1996) Conformational analysis of D1 dopamine receptor agonists: pharmacophore assessment and receptor mapping. J Med Chem 39(1):285–296. https://doi.org/10.1021/jm9502100
7. Alkorta I, Villar HO (1993) Considerations on the recognition of the D1 receptor by agonists. J Comput Aided Mol Des 7(6):659–670. https://doi.org/10.1007/BF00125324
8. Cueva JP, Giorgioni G, Grubbs RA, Chemel BR, Watts VJ, Nichols DE (2006) Trans-2,3-dihydroxy-6a,7,8,12b-tetrahydro-6H-chromeno[3,4-c]isoquinoline: synthesis, resolution, and preliminary pharmacological characterization of a new dopamine D1 receptor full agonist. J Med Chem 49(23):6848–6857. https://doi.org/10.1021/jm0604979
9. Negash K, Nichols DE, Watts VJ, Mailman RB (1997) Further definition of the D1 dopamine receptor pharmacophore: synthesis of trans-6,6a,7,8,9,13b-hexahydro-5h-benzo[d]naphth[2,1-b]azepines as rigid analogues of β-phenyldopamine. J Med Chem 40(14):2140–2147. https://doi.org/10.1021/jm970157a
10. Pettersson I, Liljefors T (1987) Structure-activity relationships for apomorphine congeners. Conformational energies vs. biological activities. J Comput Aided Mol Des 1(2):143–152. https://doi.org/10.1007/BF01676958
11. Tonani R, Dunbar Jr J, Edmonston B, Marshall GR (1987) Computer-aided molecular modeling of a D2-agonist dopamine pharmacophore. J Comput Aided Mol Des 1(2):121–132. https://doi.org/10.1007/BF01676956
12. Mewshaw RE, Kavanagh J, Stack G, Marquis KL, Shi X, Kagan MZ, Webb MB, Katz AH, Park A, Kang YH, Abou-Gharbia M, Scerni R, Wasik T, Cortes-Burgos L, Spangler T, Brennan JA, Piesla M, Mazandargmi H, Cockett MI, Ochalski R, Coupet J,

Andree TH (1997) New generation dopaminergic agents. 1. Discovery of a novel scaffold which embraces the D2 agonist pharmacophore. Structure-activity relationships of a series of 2-(aminomethyl)chromans. J Med Chem 40(26):4235–4256. https://doi.org/10.1021/jm9703653

13. Chidester CG, Lin CH, Lahti RA, Haadsma-Svensson SR, Smith MW (1993) Comparison of 5-HT1A and dopamine D2 pharmacophores. X-ray structures and affinities of conformationally constrained ligands. J Med Chem 36(10):1301–1315
14. Alkorta I, Villar HO (1994) Molecular electrostatic potential of d1 and d2 dopamine agonists. J Med Chem 37(1):210–213
15. Wilcox RE, Tseng T, Brusniak MYK, Ginsburg B, Pearlman RS, Teeter M, Durand C, Starr S, Neve KA (1998) CoMFA-based prediction of agonist affinities at recombinant D1 vs D2 dopamine receptors. J Med Chem 41(22):4385–4399. https://doi.org/10.1021/jm9800292
16. El Aouad N, Berenguer I, Romero V, Marín P, Serrano A, Andujar S, Suvire F, Bermejo A, Ivorra MD, Enriz RD, Cabedo N, Cortes D (2009) Structure-activity relationship of dopaminergic halogenated 1-benzyl-tetrahydroisoquinoline derivatives. Eur J Med Chem 44(11):4616–4621. https://doi.org/10.1016/j.ejmech.2009.06.033
17. Berenguer I, Aouad NE, Andujar S, Romero V, Suvire F, Freret T, Bermejo A, Ivorra MD, Enriz RD, Boulouard M, Cabedo N, Cortes D (2009) Tetrahydroisoquinolines as dopaminergic ligands: 1-butyl-7-chloro-6-hydroxy-tetrahydroisoquinoline, a new compound with antidepressant-like activity in mice. Bioorg Med Chem 17(14):4968–4980. https://doi.org/10.1016/j.bmc.2009.05.079
18. Andujar S, Suvire F, Berenguer I, Cabedo N, Marin P, Moreno L, Dolores Ivorra M, Cortes D, Enriz RD (2012) Tetrahydroisoquinolines acting as dopaminergic ligands. A molecular modeling study using MD simulations and QM calculations. J Mol Model 18(2):419–431. https://doi.org/10.1007/s00894-011-1061-0
19. Angelina E, Andujar S, Tosso RD, Enriz RD, Peruchena N (2014) Non-covalent interactions in receptor–ligand complexes. A study based on the electron charge density. J Phys Org Chem 27:128–134
20. Parraga J, Cabedo N, Andujar S, Piqueras L, Moreno L, Galan A, Angelina E, Enriz RD, Ivorra MD, Sanz MJ, Cortes D (2013) 2,3,9- and 2,3,11-trisubstituted tetrahydroprotoberberines as D2 dopaminergic ligands. Eur J Med Chem 68:150–166
21. Andujar SA, de Angel BM, Charris JE, Israel A, Suarez-Roca H, Lopez SE, Garrido MR, Cabrera EV, Visbal G, Rosales C, Suvire FD, Enriz RD, Angel-Guio JE (2008) Synthesis, dopaminergic profile, and molecular dynamics calculations of N-aralkyl substituted 2-aminoindans. Bioorg Med Chem 16(6):3233–3244
22. Párraga J, Andujar SA, Rojas S, Gutierrez LJ, El Aouad N, Sanz MJ, Enriz RD, Cabedo N, Cortes D (2016) Dopaminergic isoquinolines with hexahydrocyclopenta[ij]-isoquinolines as D2 −like selective ligands. Eur J Med Chem 122:27-42. https://doi.org/10.1016/j.ejmech.2016.06.009
23. Galán A, Moreno L, Párraga J, Serrano Á, Sanz MJ, Cortes D, Cabedo N (2013) Novel isoquinoline derivatives as antimicrobial agents. Bioorg Med Chem 21(11):3221–3230. https://doi.org/10.1016/j.bmc.2013.03.042
24. Malo M, Brive L, Luthman K, Svensson P (2010) Selective pharmacophore models of dopamine D1 and D2 full agonists based on extended pharmacophore features. ChemMedChem 5(2):232–246. https://doi.org/10.1002/cmdc.200900398
25. Lan H, DuRand CJ, Teeter MM, Neve KA (2006) Structural determinants of pharmacological specificity between D 1 and D2 dopamine receptors. Mol Pharmacol 69(1):185–194. https://doi.org/10.1124/mol.105.017244
26. Neve KA, Cumbay MG, Thompson KR, Yang R, Buck DC, Watts VJ, Durand CJ, Teeter MM (2001) Modeling and mutational analysis of a putative sodium-binding pocket on the dopamine D2 receptor. Mol Pharmacol 60(2):373–381
27. Kalani MYS, Vaidehi N, Hall SE, Trabanino RJ, Freddolino PL, Kalani MA, Floriano WB, Wai Tak Kam V, Goddard Iii WA (2012) The predicted 3D structure of the human D2 dopamine receptor and the binding site and binding affinities for agonists and antagonists. Proc Natl Acad Sci USA 101:3815–3820
28. Becker OM, Marantz Y, Shacham S, Inbal B, Heifetz A, Kalid O, Bar-Haim S, Warshaviak D, Fichman M, Noiman S (2004) G protein-coupled receptors: in silico, drug discovery in 3D. Proc Natl Acad Sci USA 101(31):11304–11309. https://doi.org/10.1073/pnas.0401862101
29. Micheli F, Bonanomi G, Blaney FE, Braggio S, Capelli AM, Checchia A, Curcuruto O, Damiani F, Di Fabio R, Donati D, Gentile G, Gribble A, Hamprecht D, Tedesco G, Terreni S, Tarsi L, Lightfoot A, Stemp G, MacDonald G, Smith A, Pecoraro M, Petrone M, Perini O, Piner J, Rossi T, Worby A, Pilla M, Valerio E, Griffante C, Mugnaini M, Wood M, Scott C, Andreoli M, Lacroix L, Schwarz A, Gozzi A, Bifone A, Ashby Jr CR, Hagan JJ, Heidbreder C (2007) 1,2,4-Triazol-3-yl-thiopropyl-tetrahydrobenzazepines: a series of potent and selective dopamine D3 receptor antagonists. J Med Chem 50(21):5076–5089. https://doi.org/10.1021/jm0705612
30. Párraga J, Cabedo N, Andujar S, Piqueras L, Moreno L, Galán A, Angelina E, Enriz RD, Ivorra MD, Sanz MJ, Cortes D (2013) 2,3,9- and 2,3,11-Trisubstituted tetrahydroprotoberberines as D2 dopaminergic ligands. Eur J Med Chem. 68:150-166. https://doi.org/10.1016/j.ejmech.2013.07.036
31. Angelina E, Andujar S, Moreno L, Garibotto F, Párraga J, Peruchena N, Cabedo N, Villecco M, Cortes D, Enriz RD (2015) 3-chlorotyramine acting as ligand of the D2 dopamine receptor. Molecular modeling, synthesis and D2 receptor affinity. Molec Inform 34 (1):28-43. https://doi.org/10.1002/minf.201400093
32. Morris GM, Huey R, Lindstrom W, Sanner MF, Belew RK, Goodsell DS, Olson AJ (2009) AutoDock4 and AutoDockTools4: automated docking with selective receptor flexibility. J Comput Chem 30(16):2785–2791
33. Lindorff-Larsen K, Piana S, Palmo K, Maragakis P, Klepeis JL, Dror RO, Shaw DE (2010) Improved side-chain torsion potentials for the amber ff99SB protein force field. Proteins 78(8):1950–1958. https://doi.org/10.1002/prot.22711
34. Wang J, Wolf RM, Caldwell JW, Kollman PA, Case DA (2004) Development and testing of a general amber force field. J Comput Chem 25(9):1157–1174
35. Case DA, Darden TA, Cheatham III TE, Simmerling CL, Wang J, Duke RE, Luo R, Walker RC, Zhang W, Merz KM, Roberts B, Hayik S, Roitberg A, Seabra G, Swails J, Goetz AW, Kolossváry I, Wong KF, Paesani F, Vanicek J, Wolf RM, Liu J, Wu X, Brozell SR, Steinbrecher T, Gohlke H, Cai Q, Ye X, Wang J, Hsieh M-J, Cui G, Roe DR, Mathews DH, Seetin MG, Salomon-Ferrer R, Sagui C, Babin V, Luchko T, Gusarov S, Kovalenko A, Kollman PA (2012) AMBER12. University of California, San Francisco
36. Ryckaert JP, Ciccotti G, Berendsen HJC (1977) Numerical integration of the cartesian equations of motion of a system with constraints: molecular dynamics of n-alkanes. J Comput Phys 23(3):327–341. https://doi.org/10.1016/0021-9991(77)90098-5
37. Izaguirre JA, Catarello DP, Wozniak JM, Skeel RD (2001) Langevin stabilization of molecular dynamics. J Chem Phys 114(5):2090–2098. https://doi.org/10.1063/1.1332996
38. Essmann U, Perera L, Berkowitz M, Darden T, Lee H, Pedersen L (1995) A smooth particle mesh Ewald method. J Chem Phys 103:8577–8593
39. Hou T, Li N, Li Y, Wang W (2012) Characterization of domain-peptide interaction interface: prediction of SH3 domain-mediated protein-protein interaction network in yeast by generic structure-based models. J Proteome Res 11(5):2982–2995
40. Gohlke H, Kiel C, Case DA (2003) Insights into protein-protein binding by binding free energy calculation and free energy

decomposition for the Ras-Raf and Ras-RalGDS complexes. J Mol Biol 330(4):891–913

41. Frisch MJ, Trucks GW, Schlegel HB, Scuseria GE, Robb MA, Cheeseman JR, Scalmani G, Barone V, Mennucci B, Petersson GA, Nakatsuji H, Caricato M, Li X, Hratchian HP, Izmaylov AF, Bloino J, Zheng G, Sonnenberg JL, Hada M, Ehara M, Toyota K, Fukuda R, Hasegawa J, Ishida M, Nakajima T, Honda Y, Kitao O, Nakai H, Vreven T, Montgomery JA, Jr., Peralta JE, Ogliaro F, Bearpark M, Heyd JJ, Brothers E, Kudin KN, Staroverov VN, Kobayashi R, Normand J, Raghavachari K, Rendell A, Burant JC, Iyengar SS, Tomasi J, Cossi M, Rega N, Millam JM, Klene M, Knox JE, Cross JB, Bakken V, Adamo C, Jaramillo J, Gomperts R, Stratmann RE, Yazyev O, Austin AJ, Cammi R, Pomelli C, Ochterski JW, Martin RL, Morokuma K, Zakrzewski VG, Voth GA, Salvador P, Dannenberg JJ, Dapprich S, Daniels AD, Farkas Ö, Foresman JB, Ortiz JV, Cioslowski J, Fox DJ (2009) Gaussian 09 revision D.01. Gaussian Inc, Wallingford
42. Bader RFW (1994) Atoms in molecules: a quantum theory. Clarendon, Oxford
43. Lu T, Chen F (2012) Multiwfn: a multifunctional wavefunction analyzer. J Comput Chem 33(5):580–592
44. Case DA, Cheatham Iii TE, Darden T, Gohlke H, Luo R, Merz Jr KM, Onufriev A, Simmerling C, Wang B, Woods RJ (2005) The amber biomolecular simulation programs. J Comput Chem 26(16): 1668–1688. https://doi.org/10.1002/jcc.20290
45. Angel Guio JE, Santiago A, Rossi R, Migliore de Angel B, Barolo S, Andujar S, Hernandez V, Rosales C, Charris JE, Suarez-Roca H, Israel A, Ramirez MM, Ortega J, Cano NH, Enriz RD (2011) Synthesis and preliminary pharmacological evaluation of methoxilated indoles with possible dopaminergic central action. Lat Am J Pharm 30(10):1934
46. Andujar SA, Tosso RD, Suvire FD, Angelina E, Peruchena N, Cabedo N, Cortes D, Enriz RD (2012) Searching the "biologically relevant" conformation of dopamine: a computational approach. J Chem Inf Model 52(1):99–112. https://doi.org/10.1021/ci2004225
47. Sealfon SC, Chi L, Ebersole BJ, Rodic V, Zhang D, Ballesteros JA, Weinstein H (1995) Related contribution of specific helix 2 and 7 residues to conformational activation of the serotonin 5-HT2A receptor. J Biol Chem 270(28):16683–16688
48. Trzaskowski B, Latek D, Yuan S, Ghoshdastider U, Debinski A, Filipek S (2012) Action of molecular switches in GPCRs - theoretical and experimental studies. Curr Med Chem 19(8):1090–1109. https://doi.org/10.2174/092986712799320556
49. Tosso RD, Andujar SA, Gutierrez L, Angelina E, Rodriguez R, Nogueras M, Baldoni H, Suvire FD, Cobo J, Enriz RD (2013) Molecular modeling study of dihydrofolate reductase inhibitors. Molecular dynamics simulations, quantum mechanical calculations, and experimental corroboration. J Chem Inf Model 53(8): 2018–2032
50 Ortiz JE, Pigni NB, Andujar SA, Roitman G, Suvire FD, Enriz RD, Tapia A, Bastida J, Feresin GE (2016) Alkaloids from Hippeastrum Argentinum and their cholinesterase-inhibitory activities: an in vitro and in Silico study. J Nat Prod 79(5):1241–1248. https://doi.org/10.1021/acs.jnatprod.5b00785
51 Luchi AM, Angelina EL, Andujar SA, Enriz RD, Peruchena NM (2016) Halogen bonding in biological context: a computational study of D2 dopamine receptor. J Phys Org Chem 29 (11):645-655. https://doi.org/10.1002/poc.3586